Geomechanics and Engineering, *Vol. 41, No. 6 (2025) 641-655*
https://doi.org/10.12989/gae.2025.41.6.641

A combine approach of soft computing and system reliability using sequential compounding method for geogrid reinforced retaining wall analysis

Pratima Kumari*, Pijush Samui[a] and Avijit Burman[b]

Department of Civil Engineering, National Institute of Technology Patna, Patna, Bihar 800005, India

(*Received December 21, 2024, Revised March 7, 2025, Accepted May 20, 2025*)

Abstract. This study integrates machine learning (ML) algorithms and system reliability analysis to assess the stability of geotextile-reinforced retaining walls. The research utilized ensemble-based ML techniques such as Random Forest (RF), Gradient Boosting (GBM), and Extreme Gradient Boosting (XGB), alongside the First-Order Second Moment (FOSM) method, the study evaluates multiple failure scenarios sliding, overturning, bearing capacity, rupture, and pullout with soil parameters treated as random and geometric parameters as deterministic. Results indicate that RF and GBM outperform XGB, achieving R^2 values above 85% and accuracy exceeding 90%, ensuring reliable predictions. GBM demonstrates the highest predictive accuracy, while XGB exhibits variability, particularly in sliding and rupture conditions, suggesting sensitivity to data distribution. Lower RMSE and RSR values for RF and GBM confirm minimal errors, while a Willmott Index (WI) above 0.99 reflects strong agreement between predicted and actual values. The Bias Factor remains close to 1.0, ensuring unbiased estimations, while low TIC and sMAPE values highlight superior generalization between training and testing datasets. System reliability analysis reveals a system reliability index (β_{system} = 1.083), lower than the minimum component reliability index (β_{min} = 1.213) from FOSM, emphasizing the need for a comprehensive probabilistic assessment. The study demonstrates that machine learning, particularly GBM and RF, provides robust predictions, improving the reliability evaluation of reinforced retaining walls.

Keywords: GBM; retaining wall; RF; sequential compounding method; system reliability; XGB

1. Introduction

In geotechnical engineering, geosynthetics are utilized to strengthen the mechanical properties of soil, especially by enhancing tensile resistance. These materials are often employed in projects like retaining walls, slope stabilization, and foundation support. Adding layers of geotextiles helps bind the soil into a cohesive mass, which improves the stability of the overall structure. Geosynthetics are extensively used in retaining walls and slope stabilization projects. Madhavi Latha and Rajagopal (2007) conducted a two-dimensional numerical study on geotextile-reinforced slopes, which led to the development of guidelines for selecting appropriate backfill reinforcement materials. By conducting numerical analyses, Hatami and Witthoeft (2008) examined the advantages of incorporating compressible geofoam behind the reinforced zone of earth walls. Their study revealed that geofoam could lower the maximum lateral earth pressure by 50%, contingent upon the thickness and stiffness of the geotextile. Chen *et al.* (2013) performed a numerical analysis on various layouts of geotextile-reinforced walls, concluding that geotextiles mitigate wall deformations and shrink the potential slip zone. Ardah *et al.* (2021) used a two-dimensional finite-element model to study geosynthetic-reinforced soil-integrated bridge systems and determined that their performance is largely influenced by the internal friction angle of the backfill material. Djabri and Benmebarek (2016) applied the finite-element method to evaluate the influence of spacing between two back-to-back geosynthetic retaining walls under static conditions. Khorsandiardebili and Ghazavi (2022) introduced an innovative analytical framework based on the limit state method to assess the internal stability of geocell-reinforced slopes under pseudostatic conditions. Meanwhile, Nunes *et al.* (2022) utilized numerical simulations to investigate the influence of suction profiles on the stability of geogrid-reinforced soil walls. Furthermore, Johari and Elyasi (2024) examines the reliability of geotextile-reinforced retaining walls through the jointly distributed random variables (JDRV) approach, which provides a faster alternative to Monte Carlo Simulation (MCS). Utilizing limit equilibrium methods, the study determines that internal friction angle plays a crucial role in stability assessment. Furthermore, Khosravi-Hajivand and Johri (2024) employed the Random Finite Element Method (RFEM) to analyze the stability of unsaturated soil nailing wall systems, emphasizing the influence of soil heterogeneity, suction, and elasticity modulus. The results show that although suction and elasticity improve stability, they might lead to a reduction in the system's reliability index.

Over the past few years, soft techniques have emerged as reliable and adaptable solutions for resolving challenging

*Corresponding author, Ph.D. Student
E-mail: pratimak.ph23.ce@nitp.ac.in
[a]Professor
[b]Associate Professor

Copyright © 2025 Techno-Press, Ltd.

ISSN: 2005-307X (Print), 2092-6219 (Online)

engineering problems, particularly in predicting geotechnical characteristics and analysing structural behaviour (Chandwani *et al.* 2013, Ray *et al.* 2022, Jitchaijaroen *et al*. 2024, Sabri *et al*. 2024). Sharma et al. (2019) explores artificial neural network (ANN) and genetic programming GP) for predicting dynamic responses in geogrid-reinforced foundation beds, highlighting GP's superior accuracy, sensitivity analysis, input variables, and machine learning's geotechnical applications. Momeni *et al.* (2021) explores artificial intelligence (AI) method's role in predicting Geosynthetic reinforced soil (GRS) deformation, using ANN models optimized by Gravitational Search Algorithm (GSA) and particle size optimizations (PSO), with GSA showing superior accuracy. It emphasizes GRS importance, dataset construction, and predictive modelling techniques. Furthermore, Ali *et al.* (2022) studied and highlights the shortcomings of traditional pullout testing methods and illustrates how machine learning can be used to predict geosynthetic reinforced soil capacity more efficiently, confirming its accuracy through laboratory-based validation. Chien-Ta *et al.* (2024) effectively discussed the use of hybrid Least Squares Support Vector Regression (LSSVR) for estimating deformation in geogrid-reinforced soil structures. It highlights the integration of numerical modelling (e.g., FEM) and AI techniques like ANN with optimization algorithms. Jeyaseelan and Madhavan (2024) used several intelligence techniques such as linear regression, random forest (RF) and ANN to develop the relationship between ultimate bearing capacity and reinforcement parameters. Further, the developed model's performance was evaluated using several statistical indices such as coefficient of determinations (R^2), mean absolute percentage error (MAPE), mean squared error (MSE), and root-mean-square error (RMSE).

In geotechnical studies, the uncertainty and variability of soil resistance parameters are evident, which renders deterministic analysis with fixed values inadequate. Therefore, stochastic analysis, which accounts for these uncertainties by modelling soil parameters as random variables with specific probability distributions and statistical measures, offers a more rational approach. In geotechnical studies, various approaches have been employed to evaluate structural stability. Zevgolis and Bourdeau (2012) showed that the failure probability of typical retaining walls is not a simple linear function of deterministic safety factors (FS), leading to a shift toward stochastic analysis in slope stability studies. Keykhosropur *et al*. (2012) used 3D numerical modeling with ABAQUS to assess the performance of geosynthetic-encased systems. Johari and Khodaparast (2015) introduced the Jointly Distributed Random Variables (JDRV) approach for the seismic stability of infinite slopes, incorporating stochastic parameters such as cohesion, internal friction angle, soil unit weight and seismic coefficient modelled with truncated normal PDFs. Furthermore, Javankhoshdel and Bathurst (2016) evaluated two failure modes in geosynthetic-reinforced walls under deterministic and stochastic conditions. Lin and Liu (2017) conducted reliability analyses of soil nail walls, considering both global and sliding stabilities. Johari *et al*. (2020) extended these methods to analyze nail-reinforced walls, incorporating all failure modes and determining a single FS using system reliability analysis. Peng *et al*. (2020) explored the reliability of reinforced soil slopes by analyzing local failures in reinforcements using a standard case study. The following year, Peng *et al*. (2021) conducted a stochastic seismic analysis of geosynthetic-reinforced slopes, studying critical parameters such as reinforcement spacing and slope angle. Goswami *et al*. (2022) examined deterministic and probabilistic strategies for soil reinforcement with fibers, concluding that probabilistic methods provide a simplified yet effective way to estimate strength and deformation in fiber-reinforced soils.

This study employs innovative combinations of soft computing techniques, including Random Forest (RF), Gradient Boosting (GBM), and Extreme Gradient Boosting (XGB), alongside system reliability methods to evaluate geosynthetic retaining structures. A review of the existing literature reveals that numerous studies have focused on analysing geosynthetic structures; however, these approaches were typically applied to address individual problems in isolation. In contrast, this research integrates both soft computing methods and system reliability techniques to provide a comprehensive assessment of geosynthetic retaining walls.

2. Methodology

2.1 Deterministic analysis

In the current work, a deterministic analysis of geotextile retaining wall has been performed using an excel spreadsheet. In the initial step, inputs parameters such as angle of internal friction ($\emptyset_1$) and unit weight (γ_1) for granular backfill, as well as angle of internal friction ($\emptyset_2$), unit weight (γ_2), and cohesion (c) for foundations soil, were used to generate 100 random samples in an Excel spreadsheet based on the upper and lower values of these input parameters. Additionally, geotextile ultimate tensile strength (T_{ult}) was also considered as random variable. Thus, 100 random samples also have been generated for geotextile ultimate tensile strength. Once random samples are generated, internal and external stability factors are also calculated in a spreadsheet. The theoretical background of internal and external stability factors is discussed in following subsections.

2.2 External stability

This investigation investigated the stability of a retaining wall reinforced with geotextiles, with a focus on the reinforced zone's ability to withstand sliding, overturning, and bearing load. The research treated the geotextile length and the height of the reinforced soil area as constant parameters. Each reinforced segment was modelled as a rigid block, influencing FS calculations through lateral pressures. The recommended minimum FS values for sliding, overturning, and bearing pressure are 1.5–3.0, 3.0, and 3.0–5.0, respectively (Berg *et al*. 2009).

2.2.1 Sliding

The factor of safety (FS) for sliding, denoted as $FS_{sliding}$, is represented by the equation below (Elias *et al*. 2001, Braja M.Das 2010)

$$FS_{sliding} = \frac{(w_1 + w_2 + w_3 + \cdots + qL)tan(0.67\emptyset_1)}{0.5H^2\gamma_1 K_a} \quad (1)$$

Here, w_1 is the weight of the upper portion of the wall, given by the expression $w_1 = L_1\gamma_1 z_1$ while w_2 is the weight of the lower portion, calculated as $w_2 = L_2\gamma_2 z_2$ and so on. The Rankine earth pressure coefficient, K_a, is determined by $tan^2(0.25\pi - 0.5\emptyset_1)$ and q represents the vertical stress generated by any existing surcharge loads (Berg *et al.* 2009).

2.2.2 Overturning

When the combined moment of the forces that drive rotation around the wall's toe becomes greater than the moment of the forces that resist it, overturning is likely to happen. The FS for overturning, $FS_{overturning}$, can be calculated using the following expression (Das 2010)

$$FS_{overturning} = \frac{M_R}{M_o} = \frac{0.5(L_1w_1 + L_2w_2 + L_3w_3 + \cdots + qL^2)}{0.17H^3\gamma_1 K_a} \quad (2)$$

2.2.3 Bearing pressure

A shear rupture may develop in the soil under a foundation if the applied stress surpasses the soil's allowable bearing pressure. The FS related to the foundation's bearing capacity, referred to as FS_{BP}, can be calculated using the following equation (Elias *et al.* 2001)

$$FS_{BP} = \frac{q_u}{\sigma_0'} = \frac{(c_2N_c + 0.5\gamma_2L_2N_\gamma)}{\gamma_1H + q} \quad (3)$$

The expression for the bearing capacity factors for shallow foundation, as established by Meyerhof in 1963 (Meyerhof 1963), is presented as follows

$$N_q = tan^2(0.25\pi + 0.5\emptyset_2)e^{(\pi\tan(\emptyset_2))} \quad (4)$$

$$N_c = (N_q - 1)cot(\emptyset_2) \quad (5)$$

$$N_\gamma = 2(N_q + 1)tan(\emptyset_2) \quad (6)$$

N_c, N_γ, and N_q represent the bearing capacity coefficients that are dependent on $\emptyset_2$ (Das 2010, Luo and Das 2016).

2.3 Internal stability

For the wall to remain internally stable, the geotextile must resist rupture and protrusion effectively. Stability assessments involve computing rupture and pullout forces, with target FS values ranging from 1.3 to 1.5 (Berg *et al*. 2009).

2.3.1 Rupture

Rupture in the geotextile reinforcement occurs when the lateral pressure exerted by the soil exceeds the allowable resistance of the geotextile. The safety factor for preventing rupture of the geotextile, denoted as $FS_{Rupture}$, can be calculated using this formula (Das 2010)

$$FS_{Rupture} = \frac{\sigma_G}{S_v(\gamma_1H + q)tan^2(0.25\pi - 0.5\emptyset_1)} \quad (7)$$

where σ_G is the allowable resistance of geotextile.

2.3.2 Geotextile pull-out

In the process of pull-out assessment, at any depth, z, when the frictional resistance developed along the surfaces of the reinforcement ties is less than the force acting on the ties, pull-out failure will occur. This means the tensile force in the geotextile becomes higher than the frictional resistance between the geotextile and the surrounding soil. The pull-out FS of the geotextile, $FS_{Pullout}$ can be calculated as follows (Das 2010).

$$FS_{Pullout} = \frac{4l_l\tan(0.67\emptyset_1)}{S_vtan^2(0.25\pi - 0.5\emptyset_1)} \quad (8)$$

2.4 Soft computing method

In this study, three machine learning (ML) models such as RF, GBM, and XGB were employed to evaluate the internal and external stability of geotextile retaining structures. The stability was assessed in terms of five factors of safety (FS): $FS_{sliding}$, $FS_{overturning}$, FS_{BP}, $FS_{rupture}$, and $FS_{Pullout}$. To develop the ML models, a total of 100 datasets were utilized. Of these, 80% were allocated for training, while the remaining 20% were used for validation. The dataset division was conducted randomly, and each dataset was normalized within a range of 0 to 1 using a predefined normalization formula.

$$N = \frac{x - \min(A)}{\max(A) - \min(A)} \quad (9)$$

Here, A represents the total number of datasets, and N is the normalization factor. It is important to note that all developed models were coded in Python using the Jupyter Notebook platform. The theoretical background of all developed models is illustrated in the following subsection.

2.4.1 Random forest (RF)

RF is an ensemble method for classification and regression introduced by (Breiman 2001) at the University of California, Berkeley. In recent years, RF has gained popularity due to its advantages over other algorithms. It effectively manages data with numerous features, assesses the significance of various attributes, and typically delivers high accuracy in both classification and regression tasks, along with a quick learning process. In RF, each tree selects a small subset of features during its construction (this is the second randomization step). This approach allows RF to handle datasets with many attributes efficiently, maintaining reasonable processing times. Notably, the decision tree (DT) is constructed while keeping *m* unchanged. After generating K such trees, their results are aggregated using

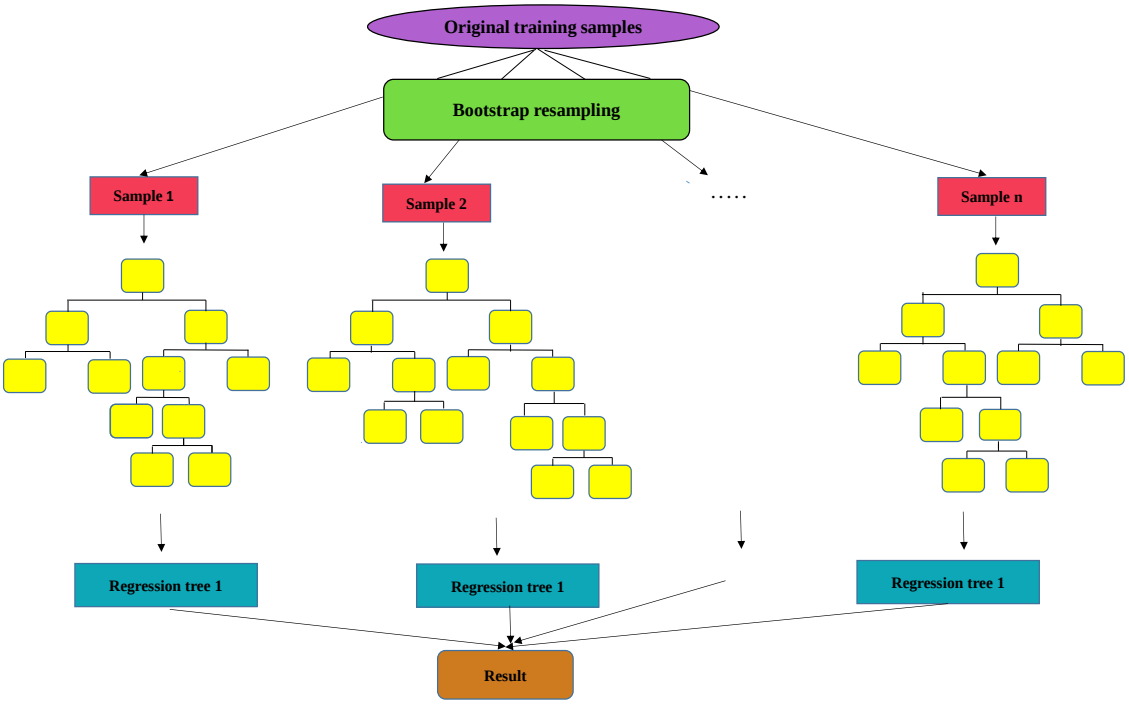

Fig. 1 Schematic view of RF algorithm

the bagging approach to obtain the final prediction, as outlined in Eq. (10).

$$\check{y} = \frac{1}{K}\sum_{K=1}^{K} h(x,\theta) \tag{10}$$

The user can set a default number of features for tree construction, with the typical recommendation being $\sqrt{P}$ for classification tasks and P/3 for regression tasks, where P is the total number of features in the dataset. To ensure that all features are utilized multiple times, a large number of trees is suggested (usually around 500) for classification and 1000 for regression problems. Because the bootstrap method is employed for random sampling with replacement, around two-thirds of the samples in each subset are unique, while the remaining one-third are repeated during tree construction. A schematic diagram of the RF model is shown in Fig. 1, demonstrating how multiple decision trees are utilized, with the final estimation being the average of their individual predictions.

2.4.2 Gradient boosting (GBM)

GBM is a stepwise algorithm designed to combine multiple weak models into a more powerful model. Its goal is to approximate a function, denoted as $f^*(x)$, that links input data x to target values y within a dataset $S = \{(x_i, y_i)\}_{i=1}^{n}$ where i = 1 to n, representing n observations. GBM achieves this by minimizing the expected value of a loss function, $L(y, f(x))$. The algorithm builds the additive approximation of the function $f^*(x)$ as a weighted sum of functions, as shown in Eq. (11). Here, ρ_t signifies the weight of the t[th] base learner for $t = 1, \ldots, T$.

$$f_t(x) = f_{t-1}(x) + \rho_t h_t(x) \tag{11}$$

Eq. (12) employs an iterative approach to achieve a consistent estimate of f^* where the loss function, represented as $L(y_i, \alpha)$, is differentiable.

$$f_0(x) = argmin \sum_{i=1}^{n} L(y_i, \alpha) \tag{12}$$

The primary goal of the base learners is to minimize the expression in Eq. (13). During the gradient descent optimization process for f^*, each base learner h_t takes a step in a greedy fashion (Marani and Nehdi 2020). For each model, a new dataset $S = \{(x_i, y_i)\}_{i=1}^{n}$ is trained, and the pseudo residuals r_{ti} are quantified based on Eq. (14). A line search optimization method is then applied to find the weight ρ_t. The main objective of GB is to minimize errors and improve the model's accuracy.

$$f_0(x) = argmin \sum_{i=1}^{n} L(y_i, f_{t-1}(x_i) + \rho h(x_i)) \tag{13}$$

$$r_{ti} = \left[\frac{\delta L(y_i, f(x))}{\delta f(x)}\right] \text{ where } f(x) = f_{t-1}(x) \tag{14}$$

and future contexts of the input sequence. The accuracy and

2.4.3 Extreme gradient boosting (XGB)

XGB is a highly efficient method that can flexibly handle distributed and parallel computing while managing sparse data. It offers a cutting-edge solution for tackling machine learning and data mining challenges. Compared to commercial software, XGB delivers classification results with greater accuracy and performs calculations up to 10 times faster. It also effectively handles missing values and helps prevent overfitting. Through its learning process, XGB can automatically decide the best way to split samples

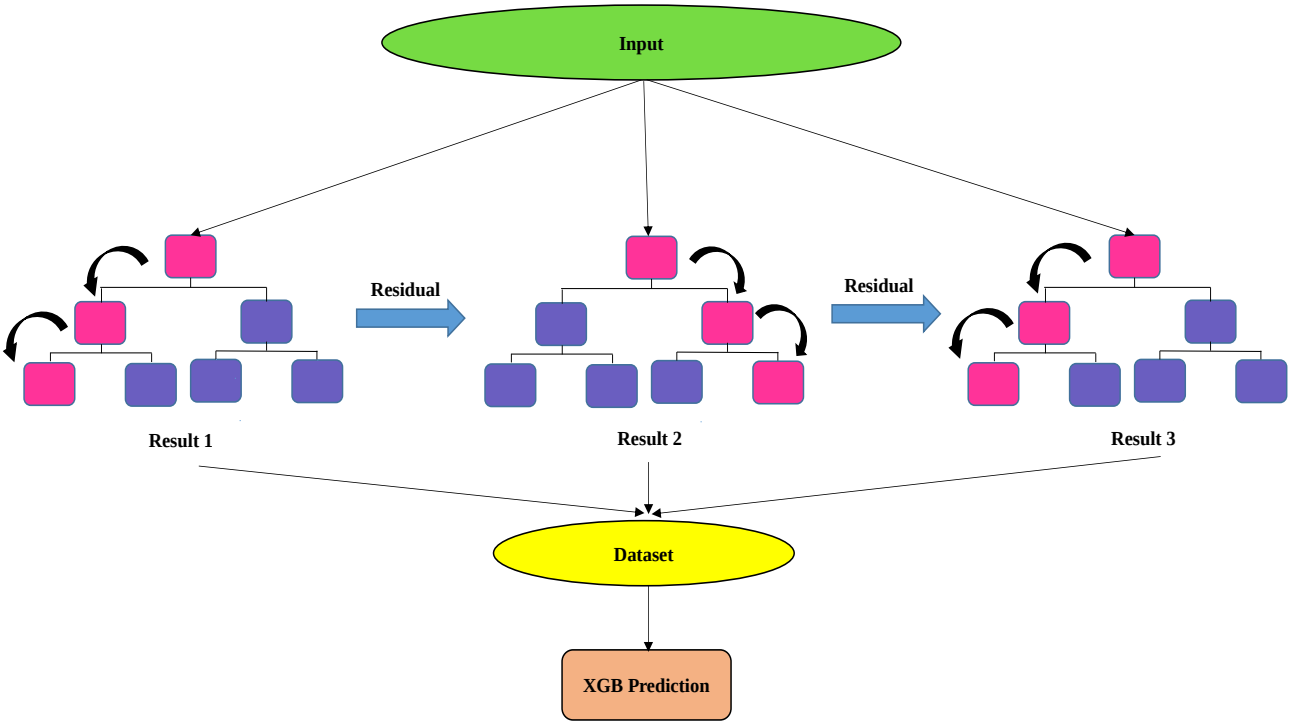

Fig. 2 Basic network of XGB

that have missing feature values (Chang *et al.* 2018). XGB, a machine learning algorithm rooted in gradient boosting trees, excels in enhancing gradient performance and offers an effective approach for solving both regression and classification tasks (Ding *et al.* 2020). The working principles of the XGB algorithm are described below:

Considering a dataset, $H = \{(x_i, y_i)\}$ with k instances and p dimensions $(|H| = k, x_i \in R^P, y_i \in R)$ the predictions for a tree ensemble model are made using M additive functions in the following manner

$$y_i = \phi(x_i) = \sum_{m=1}^{M} f_m(x_i), f_m \in S \tag{15}$$

In this context, F refers to the regression tree space and is determined as

$$S = \left\{ f(x) = w_{b_{(x)}} \right\} (b: R^p \to T, w \in R^T) \tag{16}$$

In this case, b corresponds to the tree structure, T denotes the leaves in the tree, and f_m is a function determined by b and the leaf weights w. To lower errors within the trees, the XGB model determines the minimization function

$$L^t = \sum_{k=1}^{k} l\left(y_i, \tilde{y}_i^{(t-1)} + f_t(x_i)\right) + \Omega(f_t) \tag{17}$$

Here, l denotes a convex objective function measuring the dissimilarity between predicted $\tilde{y}_i$ and actual y_i values; t indicates the number of cycles to reduce errors; and Ω captures the complexity of the regression tree functions. The schematic diagram of XGB was shown in Fig. 2.

2.5 Quantitative indicator

To validate the accuracy of the developed models, a set of ten statistical metrics was applied. These comprised the coefficient of determination (R^2), root mean square error (RMSE), RMSE/SD ratio (RSR), Willmott's index of agreement (WI), bias factor, Legate and McCabe's index (LMI), index of agreement, symmetric mean absolute percentage error (sMAPE), and Theil's inequality coefficient (TIC), drawing from earlier studies (Jaiswal *et al.* 2024, Sabri *et al.* 2024, Hwang *et al.* 2024). The equations for these metrics and their ideal values are tabulated in Table 1. The variable N represents the overall datasets incorporated in the model, y_i and $y_{i_{pre}}$ signify the observed and forecasted UCS values, respectively, while y_{avg} is the average of the observed data. Ideally, these statistical indicators should closely resemble their theoretical benchmarks, as outlined in earlier publications (Khandelwal and Singh 2006, Bardhan *et al.* 2022, Kardani *et al.* 2022)

2.6 Reliability index

Uncertainties in soil parameters can be systematically integrated into geotechnical assessments using probability theory and statistical methods. In this technique, the performance of geotechnical structures is evaluated in terms of probability, often using the reliability index (β) or the probability of failure (POF) as indicators. The POF represents the chance that the structure will not meet the required performance standards. In the current work, first-order second-moment method (FOSM) has been used to find the β. The mathematical expressions related to FOSM techniques are presented in Eq. (28).

Table 1 Overview of quantitative expression metrics and their corresponding ideal values

Expression	Ideal Value	Equations
$R^2 = \frac{\sum_{i=1}^{n}(y_i - y_{avg})^2 - \sum_{i=1}^{n}(y - \widehat{y_i})^2}{\sum_{i=1}^{n}(y_i - y_{avg})^2}$	1	(18)
$RMSE = \sqrt{\frac{1}{n}\sum_{i=1}^{n}(y_i - \bar{y}_i)^2}$	0	(19)
$RSR = \frac{RMSE}{\sqrt{\frac{1}{n}\sum_{i=1}^{n}(y_i - y_{avg})^2}}$	0	(20)
$WI = 1 - \left[\frac{\sum_{i=1}^{n}(y_i - y_{i_{pre}})^2}{\sum_{i=1}^{n}\{\lvert y_i - y_{avg}\rvert + \lvert y_i - y_{avg}\rvert\}^2}\right]$	1	(21)
$Bias\ Factor = \frac{1}{N}\sum_{i=1}^{N}\frac{y_i}{y_{i_{pre}}}$	0	(22)
$LMI = 1 - \left[\frac{\sum_{i=1}^{N}\lvert y_i - y_{i_{pre}}\rvert}{\sum_{i=1}^{N}\lvert y_i - \bar{y}_{i_{pre}}\rvert}\right]$	1	(23)
$t - stat = \sqrt{\frac{(N-1)MBE^2}{(RMSE)^2 - MBE)}}$	0	(24)
$\mathrm{IA} = \left[\frac{\sum_{i=1}^{N}(y_{i_{pre}} - y_i)^2}{\sum_{i=1}^{N}\left\{\lvert y_i - y_{avg}\rvert + \lvert y_{i_{pre}} - y_{avg}\rvert\right\}^2}\right]$	0	(25)
$sMAPE = \frac{2}{N}\sum_{i=1}^{n}\frac{\lvert y_i - y_{i_{pre}}\rvert}{\lvert y_i\rvert + \lvert y_{i_{pre}}\rvert}$	0	(26)
$\mathrm{TIC} = \frac{\sqrt{\frac{1}{N}\sum_{i=1}^{N}(y_{i_{pre}} - y_i)^2}}{\sqrt{\frac{1}{N}\sum_{i=1}^{N}y_{i_{pre}}^2} + \sqrt{\frac{1}{N}\sum_{i=1}^{N}y_i^2}}$	0	(27)

$$\beta = \frac{\mu_{FS} - 1}{\sigma_{FS}} \tag{28}$$

Here, μ_{FS} and σ_{FS} are the mean and standard deviation of the FOS, respectively.

2.7 System reliability

In this work, the external and internal stability safety factors were modelled as stochastic output variables. When evaluating the overall stability of a geotechnical system, it is important to consider the interaction between the stability factors of each component. This interaction can be analysed using stochastic methods by calculating the reliability index. As a result, the reliability index (β) for the geotextile-reinforced retaining wall system is determined. For this purpose, sequential compounding method (SCM) has been used to conduct system reliability.

2.7.1 Sequential compounding method

This method initially calculates the reliability of individual components, then progressively combines them in pairs to create equivalent components, ultimately working towards the system's overall reliability. This approach addresses the challenges faced by previous methods. A key advantage of SCM is that each process involves only two components, which simplifies the logical operations compared to other methods (Genz 2004, Kang and Song 2010, Xing *et al.* 2021).

By applying the union operation between two components, E_1 and E_2, a compound event, $E_{1or\,2}$, can be created. The reliability index for this compound event, $\beta_{1\,or\,2}$, is first determined by exploiting the symmetry inherent in standard normal distribution.

$$\begin{aligned}\beta_{1\,or\,2} &= -\phi^{-1}[P(E_1 \cup E_2)] \\ &= \phi^{-1}\left[\phi(\beta_1)\phi(\beta_2) + \int_0^{\rho\,1,2}\varphi(\beta_1,\beta_2;\rho)d\rho\right]\end{aligned} \tag{29}$$

where

$$\begin{aligned}&\int_0^{\rho\,1,2}\varphi(\beta_1,\beta_2,\rho)\,d\rho \\ &= \int_0^{\rho\,1,2}\frac{1}{2\pi\sqrt{1-\rho_{1,2}^2}}exp\left(\frac{-1}{2(1-\rho_{1,2}^2)}\left(\beta_1{}^2 + \beta_2{}^2 - 2\beta_1\beta_2\right)\right)\end{aligned} \tag{30}$$

Here, ϕ indicates the marginal cumulative distribution function (CDF) of the standard normal distribution, and φ is the probability density function (PDF) of the standard normal distribution. The reliability indices of events E_1 and E_2 are represented by β_1 and β_2, while $\rho_{1,2}$ is the correlation coefficient between the standard normal random variables z_1 and z_2, associated with E_1 and E_2. To determine the correlation coefficients between the new compound event E_1 or E_2 and the remaining events in the system, it is necessary to employ decomposition and approximation methods for conditional probabilities as described below.

$$\Phi\left(-\beta_{(1\,or\,2)|k}\right) = 1 - \Phi_2\left(\beta_{1|k}, \beta_{2|k}, \rho_{1,2|k}\right) \tag{31}$$

Upon simplification, the above expression can be rewritten as

$$\begin{aligned}&\Phi\left(-\beta_{(1\,or\,2)|k}\right) \\ &= 1 - \Phi\left(\beta_{1|k}\right)\Phi\left(\beta_{2|k}\right) \\ &+ \int_0^{\rho\,1,2|k}\frac{1}{2\pi\sqrt{1-\rho_{1,2}^2}}exp\left(\frac{-1}{2(1-\rho_{1,2}^2)}\left(\beta_1{}^2 + \beta_2{}^2 - 2\beta_1\beta_2\rho\right)\right)\end{aligned} \tag{32}$$

From Eqs. (33)-(35), $\beta_{1|k}$, $\beta_{2|k}$ and $\rho_{1,2|k}$ are calculated by following expression

$$\beta_{1|k} = \frac{\left(\beta_1 - \rho_{1,k}A\right)}{\sqrt{1-\rho_{1,k}^2 B}} \tag{33}$$

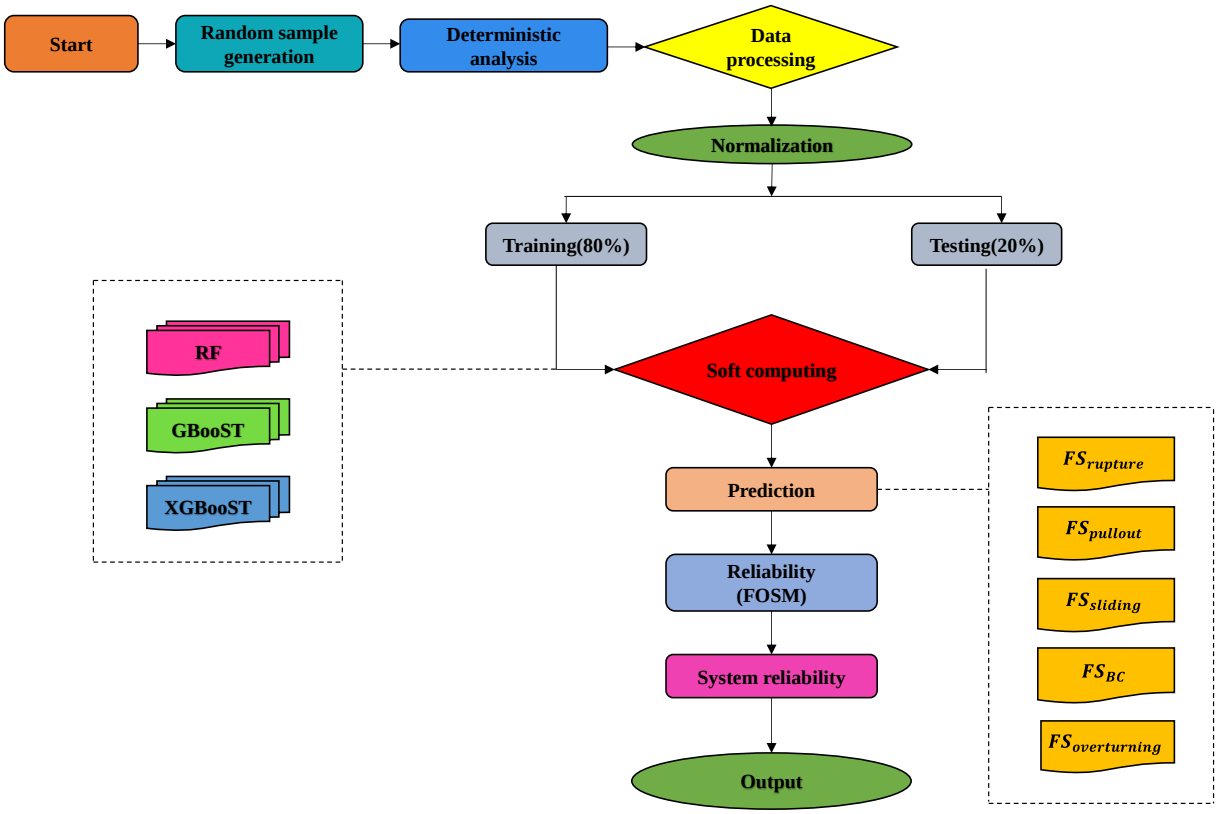

Fig. 3 Workflow for system reliability

$$\beta_{2|k} = \frac{(\beta_2 - \rho_{2,k}A)}{\sqrt{1-\rho_{2,k}^2 B}} \tag{34}$$

$$\rho_{1,2|k} = \frac{(\rho_{1,2} - \rho_{1,k}\rho_{2,k}B)}{\sqrt{1-\rho_{1,k}^2 B}\sqrt{1-\rho_{2,k}^2 B}} \tag{35}$$

$$\beta_{(1\text{ or }2)|k} = (\beta_{(1\text{ or }2)} - \rho_{(1\text{ or }2),k}A)/\sqrt{1-\rho_{(1\text{ or }2),k}^2 B} \tag{36}$$

$$A = \frac{\varphi(-\beta_k)}{\Phi(-\beta_k)} \tag{37}$$

$$B = A(-\beta_k + A) \tag{38}$$

Here, Φ_2 stands for the joint CDF of the bivariate standard normal distribution, while $\varphi(\beta_k)$ indicates the PDF of the standard normal distribution. Eq. (36) is solved numerically for each compounding iteration to determine ρ (1 or 2), where k varies from 3 to n, and n denotes the total number of components currently in the system during the sequential compounding process, adhering to the condition that $1 \leq \rho$ (1 or 2), $k \leq 1$.

2.8 Workflow of complete methodology

This section provides a comprehensive overview of the methodology employed for the application of soft computing techniques and system reliability analysis in the context of geosynthetic retaining structures. The detailed steps involved in the study are systematically outlined to ensure clarity and reproducibility. The entire workflow, encompassing data preparation, deterministic analysis, model development, analysis, validation, and system reliability are visually represented in Fig. 3, which serves as a roadmap for the study. Each phase of the methodology is meticulously designed to address the objectives of the research, integrating advanced computational techniques with reliability-based approaches to evaluate and predict the performance of geosynthetic retaining systems.

3. Case study and application

This study aims to apply soft computing techniques and system reliability analysis to geotextile retaining structures. For this, datasets were generated by varying the soil parameters within specified upper and lower bounds.

The range of these soil parameters was carefully selected to ensure the comprehensive representation of potential field conditions. Descriptive statistics for the collected data are presented in Table 3, offering an overview of the statistical distribution of the variables under investigation. It is important to note that the ultimate bearing capacity of the geotextile was taken from a previously published study (Miyata *et al.* 2018, Bathurst and Naftchali 2021), ensuring consistency with established values in the field. The illustrative geometry of the

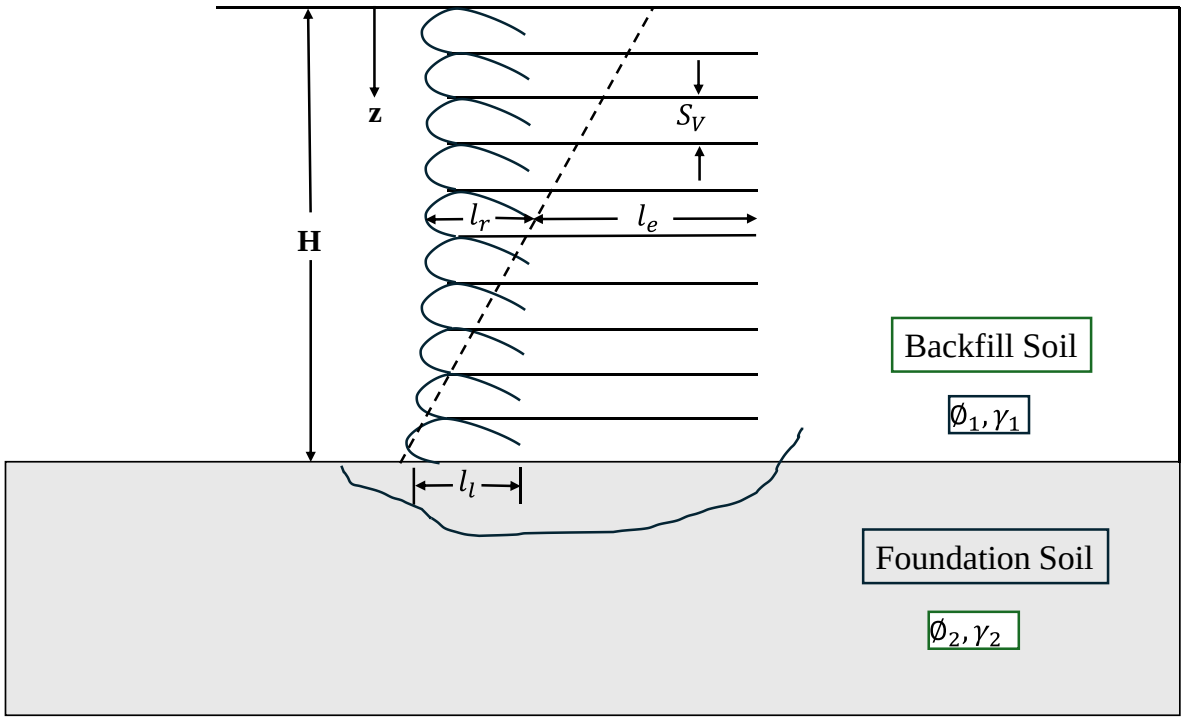

Fig. 4 Illustrative geotextile retaining structure

Table 2 Summary of deterministic input parameter

Input parameter	Unit	Value
Height (H)	m	5.0
Vertical Spacing (S_v)	m	0.5
Depth (z)	m	2.0
Length of each layer of geotextile (L)	m	3.0

Table 3 Summary of the descriptive statistics of the input random variable

Particular	$\emptyset_1$	γ_1	$\emptyset_2$	γ_2	T_{ult}
Mean	35.82	18.07	38.28	18.65	117.01
Standard Error	0.42	0.16	0.52	0.23	2.58
Median	36.06	18.03	38.53	18.36	118.33
Standard Deviation	4.24	1.64	5.15	2.27	25.79
Sample Variance	17.97	2.68	26.52	5.17	665.34
Kurtosis	0.03	0.72	-0.42	38.46	0.45
Skewness	-0.13	-0.26	-0.23	4.99	0.01
Range	20.74	8.98	23.80	21.09	139.63
Sum	3582.07	1806.78	3827.72	1864.76	11700.90
Count	100.00	100.00	100.00	100.00	100.00

geotextile reinforced retaining wall, which serves as a key component in this work, is depicted in Fig. 4. In this figure, the following parameters are presented: H is the total height of the geotextile-reinforced retaining wall, S_v is the vertical spacing of the layer at any depth z. The reinforcement length and embedment length are represented by l_r and l_e, respectively. The sum of l_r and l_e is referred to as the length of each layer of geotextile (L). The friction angles of the backfill and soil foundation are $\emptyset_1$ and $\emptyset_2$, respectively. γ_1 and γ_2 denote the unit weights of the backfill and soil foundation, while c_2 is the cohesion of the soil foundation.

3.1 Data preparation

Soil parameters are inherently uncertain, and their values can fluctuate due to their heterogeneous nature. However, these uncertainties can be addressed through probabilistic modelling. As previously mentioned, a total of 100 samples were generated in an Excel spreadsheet for $\emptyset_1$, γ_1, $\emptyset_2$, γ_2 and T_{ult}. Each random variable was varied within its defined limits (upper and lower bounds) using the formula =NORM.INV (RAND (), mean, stdev.) in Excel, which produces random values following a normal distribution. These limits were considered based on previous studies (Miyata *et al.* 2018, Bathurst and Naftchali 2021).

The descriptive statistics of generated datasets are shown in the above Table 3. It is important to note that the data generation procedure was followed based on previous studies (Mustafa *et al.* 2023, 2024, Kumar *et al.* 2023, Sabri *et al.* 2024).

After preparing the data, the geotextile retaining structure's external and internal stability was analysed, with the factor of safety (FOS) computed using Eqs. (1)-(8). Next, in computational modelling, the input and output parameters were pre-processed and normalized following Eq. (9). The full workflow of the computational modelling process has already been described in Section 2.8 of the methodology.

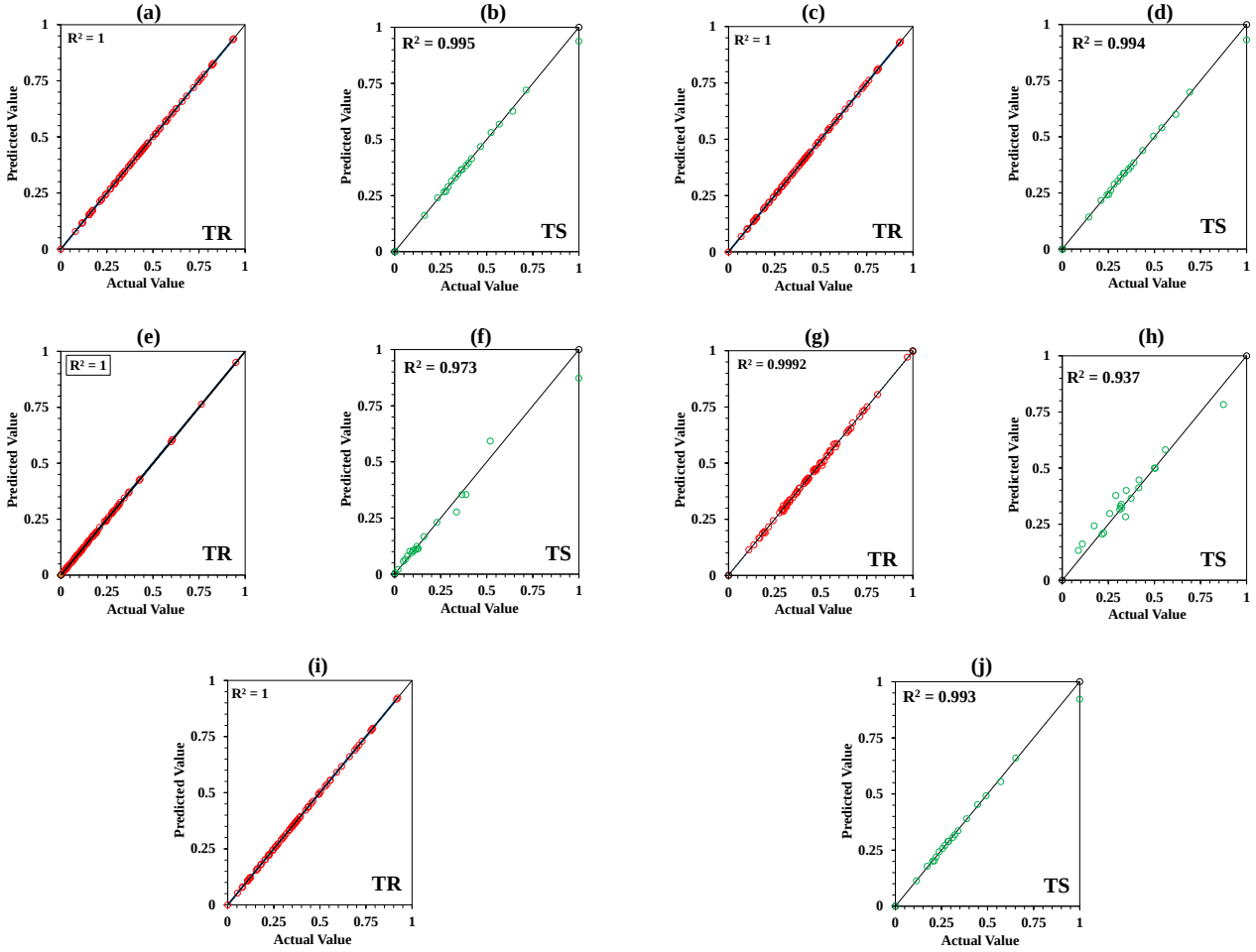

Fig. 5 Scatter plots showing the relationship between actual and predicted values using GBM model across different scenarios in the in the TR and TS stages: (a-b) Sliding, (c-d) Overturning, (e-f) Bearing pressure, (g-h) Rupture, and (i-j) Pullout

Table 4 Details of inputs and output selection during prediction

$\emptyset_1, \gamma_1$	$FS_{sliding}$
$\emptyset_1, \gamma_1$	$FS_{overturning}$
$\emptyset_2, \gamma_1, \gamma_2$	FS_{BC}
$\emptyset_1, \gamma_1, T_{ult}$	$FS_{rupture}$
$\emptyset_1$	$FS_{pullout}$

Table 5 Best hypermeter selection during development stage

Models	Hyperparameters Selection
RF	n_estimators = 100, random_state = 4, depth = 10, learning rate = 0.001
GBM	n_estimators = 100, random_state = 4, depth = 4, learning_rate = 0.001
XGB	n_estimators = 200, random_state = 4, Booster type: 'gbtree', learning_rate = 0.001

4. Results and discussion

4.1 Predictive analysis of geotextile retaining structures

This study successfully developed the three ML based models such as RF, GBM, and XGB, to predict the FS under various failure conditions, including sliding $FS_{sliding}$, overturning $FS_{overturning}$, bearing capacity FS_{BC}, rupture $FS_{rupture}$, and pullout $FS_{pullout}$. To replace traditional deterministic calculations with soft computing approaches for geotextile retaining structures, FS values were predicted using various input combinations. The input parameters and corresponding output factors are detailed in Table 4. During the development of the models, multiple combinations of tuning parameters were explored, and the optimal hyperparameters were selected to ensure accurate predictions. The hyperparameter details are provided in Table 5. Additionally, the performance of all developed models was evaluated using 10 statistical metrics during both training (TR) and testing (TS) phases. A comprehensive summary of the models' performance is presented in Table 6. A detailed summary of each model's performance, including R^2, RMSE, RSR, WI, BIAS factor, LMI, t-stat, IA, sMAPE, and TIC, for all failure conditions is provided in Table 5. The results indicate that the models

Table 6 Performance evaluation of developed models in each scenario

Models	Stages	R^2	RMSE	RSR	WI	BIAS FACTOR	LMI	t-stat	IA	sMAPE	TIC
Scenario: Sliding											
RF	TR	0.999	0.019	0.025	0.999	0.013	0.985	0.052	0.0002	0.002	0.002
	TS	0.992	0.072	0.092	0.998	0.050	0.935	0.018	0.002	0.008	0.009
GBM	TR	1.000	0.001	0.001	1.000	0.013	0.999	0.000	0.000	0.000	0.000
	TS	0.995	0.056	0.071	0.998	0.049	0.951	0.017	0.001	0.006	0.007
XGB	TR	1.000	0.004	0.005	1.000	0.013	0.995	0.054	0.0000	0.001	0.001
	TS	0.956	0.605	0.770	0.797	0.054	0.054	0.053	0.2034	0.116	0.067
Scenario: Overturning											
RF	TR	0.999	0.014	0.025	0.999	0.050	0.013	0.787	0.000	0.005	0.004
	TS	0.990	0.060	0.098	0.997	0.050	0.935	0.147	0.003	0.013	0.015
GBM	TR	1.000	0.001	0.001	1.000	0.049	0.013	0.000	0.000	0.000	0.000
	TS	0.994	0.047	0.077	0.998	0.050	0.949	0.973	0.002	0.009	0.012
XGB	TR	1.000	0.003	0.005	1.000	0.054	0.013	0.010	0.000	0.001	0.001
	TS	0.987	0.470	0.770	0.800	0.056	0.064	0.509	0.200	0.196	0.111
Scenario: Bearing Capacity											
RF	TR	0.986	0.579	0.116	0.996	0.012	0.923	1.064	0.004	0.034	0.036
	TS	0.935	0.713	0.255	0.981	0.050	0.814	0.052	0.019	0.094	0.090
GBM	TR	1.000	0.446	0.010	1.000	0.013	0.989	0.000	0.000	0.008	0.003
	TS	0.973	0.864	0.163	0.993	0.049	0.869	0.641	0.007	0.067	0.057
XGB	TR	1.000	0.216	0.005	1.000	0.012	0.996	0.730	0.000	0.004	0.001
	TS	0.866	0.651	0.366	0.952	0.047	0.513	0.822	0.048	0.237	0.138
Scenario: Rupture											
RF	TR	0.968	0.364	0.179	0.991	0.012	0.842	0.185	0.009	0.033	0.025
	TS	0.864	0.699	0.369	0.957	0.052	0.496	0.419	0.043	0.090	0.055
GBM	TR	0.999	0.058	0.029	1.000	0.013	0.972	0.000	0.000	0.007	0.004
	TS	0.937	0.474	0.250	0.982	0.051	0.715	0.351	0.018	0.063	0.037
XGB	TR	1.000	0.009	0.004	1.000	0.013	0.996	0.094	0.000	0.001	0.001
	TS	0.815	0.814	0.430	0.943	0.053	0.488	0.419	0.057	0.099	0.063
Scenario: Pullout											
RF	TR	1.000	0.087	0.020	1.000	0.012	0.987	0.096	0.000	0.005	0.004
	TS	0.989	0.472	0.105	0.997	0.050	0.941	0.574	0.003	0.016	0.021
GBM	TR	1.000	0.003	0.001	1.000	0.013	1.000	0.000	0.000	0.000	0.000
	TS	0.993	0.388	0.086	0.998	0.050	0.946	0.998	0.002	0.013	0.017
XGB	TR	1.000	0.008	0.002	1.000	0.013	0.999	0.050	0.000	0.001	0.000
	TS	0.989	0.464	0.103	0.997	0.049	0.915	0.243	0.003	0.021	0.021

performed well across different failure scenarios, with particularly strong performance seen in the training phase for all models. However, the XGB model showed notable variability in test-phase performance across different scenarios, especially for sliding and rupture conditions. To better illustrate the model's predictive accuracy, scatter plots have been provided for the best-performing model, showing the relationship between actual and predicted values in both construction and validation stage. Additionally, it is important to note that the plots are presented on a normalized scale for consistency and better interpretability.

4.2 Reliability index

This section provides a detailed analysis of the reliability of geosynthetic retaining structures under various failure conditions, utilizing the FOSM method. The reliability analysis is conducted by applying the FOSM approach, as outlined in Eq. (28), which allows for the estimation of failure probabilities by considering second-order moments of the random variables involved. Table 7 presents a comparative study of the FOSM results for predicting the reliability of geosynthetic retaining structures under different failure conditions during both the TR and TS phases. The table compares the actual reliability values (β_{actual}) with the reliability values predicted by the three machine learning models RF, GBM, and XGB for failure modes including rupture, pullout, sliding, bearing pressure, and overturning. For each failure condition, the results show a close alignment between the predicted and actual

Table 7 Comparison study of FOSM in Training and Testing Phases

Parameter	Reliability (β)	TR	TS
Rupture	β_{Actual}	2.925	2.596
	β_{RF}	3.257	3.424
	β_{GBM}	2.935	3.057
	β_{XGB}	2.931	3.408
Pullout	β_{Actual}	2.239	2.006
	β_{RF}	2.262	2.157
	β_{GBM}	2.240	2.104
	β_{XGB}	2.242	2.104
Sliding	β_{Actual}	4.172	3.891
	β_{RF}	4.214	4.135
	β_{GBM}	4.172	4.036
	β_{XGB}	4.180	5.875
Bearing Capacity	β_{Actual}	1.279	1.022
	β_{RF}	1.339	1.175
	β_{GBM}	1.280	1.095
	β_{XGB}	1.282	1.433
Overturning	β_{Actual}	1.684	1.492
	β_{RF}	1.701	1.588
	β_{GBM}	1.684	1.546
	β_{XGB}	1.688	2.548

reliability values. The RF model shows generally consistent results, with a slight overestimation of reliability during the testing phase for most scenarios. The GBM model, like RF, provides reliable predictions with minimal variation between the TR and TS phases. XGB, however, demonstrates a notable variation in the sliding failure mode, where the reliability value predicted in the testing phase is significantly higher than the actual value, indicating potential overfitting in this scenario. For better understanding, Fig. 6 presents a bar chart comparing the employed models and their predictive reliability across all scenarios in both TR and TS stages.

Overall, the FOSM method was effective in quantifying the reliability of geosynthetic retaining structures, and the developed machine learning models (RF, GBM, and XGB) showed robust performance in predicting the failure probabilities for various failure conditions, with minimal discrepancies between the TR and TS phases. These results highlight the efficacy of soft computing techniques in replacing traditional deterministic approaches for system reliability analysis in geotechnical engineering applications.

4.3 System reliability analysis

Physical systems consisting of several elements can be arranged in series, parallel, or mixed forms (Johari and Lari 2016). A series system will fail if any one component fails, whereas in a parallel system, the system will only fail if all the components experience failure. The reliability of the reinforced wall system is analysed in this section. Since a geotextile-reinforced retaining wall consists of various elements, it is crucial to consider the influence of these components on the system's overall reliability. The geotextile-reinforced wall consists of five critical components: sliding, overturning, bearing capacity, rupture, and pullout. Each of these components contributes to the overall stability of the wall, and instability in any of them can compromise the entire structure. As a result, the system is treated as a series system, necessitating the calculation of the reliability index for each component. The SCM technique was employed to combine the components and examine the correlation between them $\beta_1 = FS_{rupture}$, $\beta_2 = FS_{Pullout}$, $\beta_3 = FS_{sliding}$, $\beta_4 = FS_{BC}$, $\beta_5 = FS_{overturning}$. The correlation between the safety factors in overall actual datasets (100 datasets) conditions are shown in Eq. (39).

$$\rho = \begin{bmatrix} FS_{rupture} & FS_{Pullout} & FS_{sliding} & FS_{Bearing\ capacity} & FS_{Overtunring} & \\ 1 & 0.596597 & 0.589816 & -0.12596 & 0.59302 & FS_{rupture} \\ & 1 & 0.996112 & -0.12449 & 0.998468 & FS_{Pullout} \\ & & 1 & -0.11815 & 0.999459 & FS_{Sliding} \\ & & & 1 & -0.12076 & FS_{Bearing\ capasity} \\ & & & & 1 & FS_{Bearing\ capasity} \end{bmatrix} \quad (39)$$

To begin, the system includes two components, E_1 and E_2, associated with the reliability indices β_1 and β_2, respectively. The combined reliability index of the system, β_A, is formulated as

$$E_{1or2} = E_1 \cup E_2 = E_A = \beta_{1or2} = \beta_A = 2.158 \quad (40)$$

The subsequent step involves determining the correlation coefficient between the newly created compound event E_A and the system's remaining component events. The correlation matrix for this is as follows

$$\rho = \begin{bmatrix} 1 & 0.814636 & -0.13204 & 0.985488 \\ & 1 & -0.11815 & 0.999459 \\ & & 1 & -0.12076 \\ & & & 1 \end{bmatrix} \quad (41)$$

Next, the two components E_A and E_3 are linked together to establish a unified equivalent event E_B.

$$E_{A\,or3} = E_A \cup E_3 = E_B = \beta_{A\,or3} = \beta_B = 2.158 \quad (42)$$

Consistent with the previous method, the new correlation coefficient matrix is derived as follows

$$\rho = \begin{bmatrix} 1 & 0.99 & 0.98607 \\ & 1 & -0.12076 \\ & & 1 \end{bmatrix} \quad (43)$$

The two components E_B and E_4 are then linked at their intersection to compute a singular equivalent event EC in the next step

$$E_{B\,or4} = E_B \cup E_4 = E_C = \beta_{B\,or4} = \beta_C = 1.213 \quad (44)$$

Similarly, the new correlation matrix is as shown below

$$\rho = \begin{bmatrix} 1 & 0.544646 \\ & 1 \end{bmatrix} \quad (45)$$

In the last step, the two compound events E_C and E_5 are united to obtain the system reliability index as outlined below

$$E_{C\,or5} = E_C \cup E_5 = E_{system} = \beta_{C\,or5} = \beta_{system} = 1.083 \quad (46)$$

The method explained earlier was used to calculate the

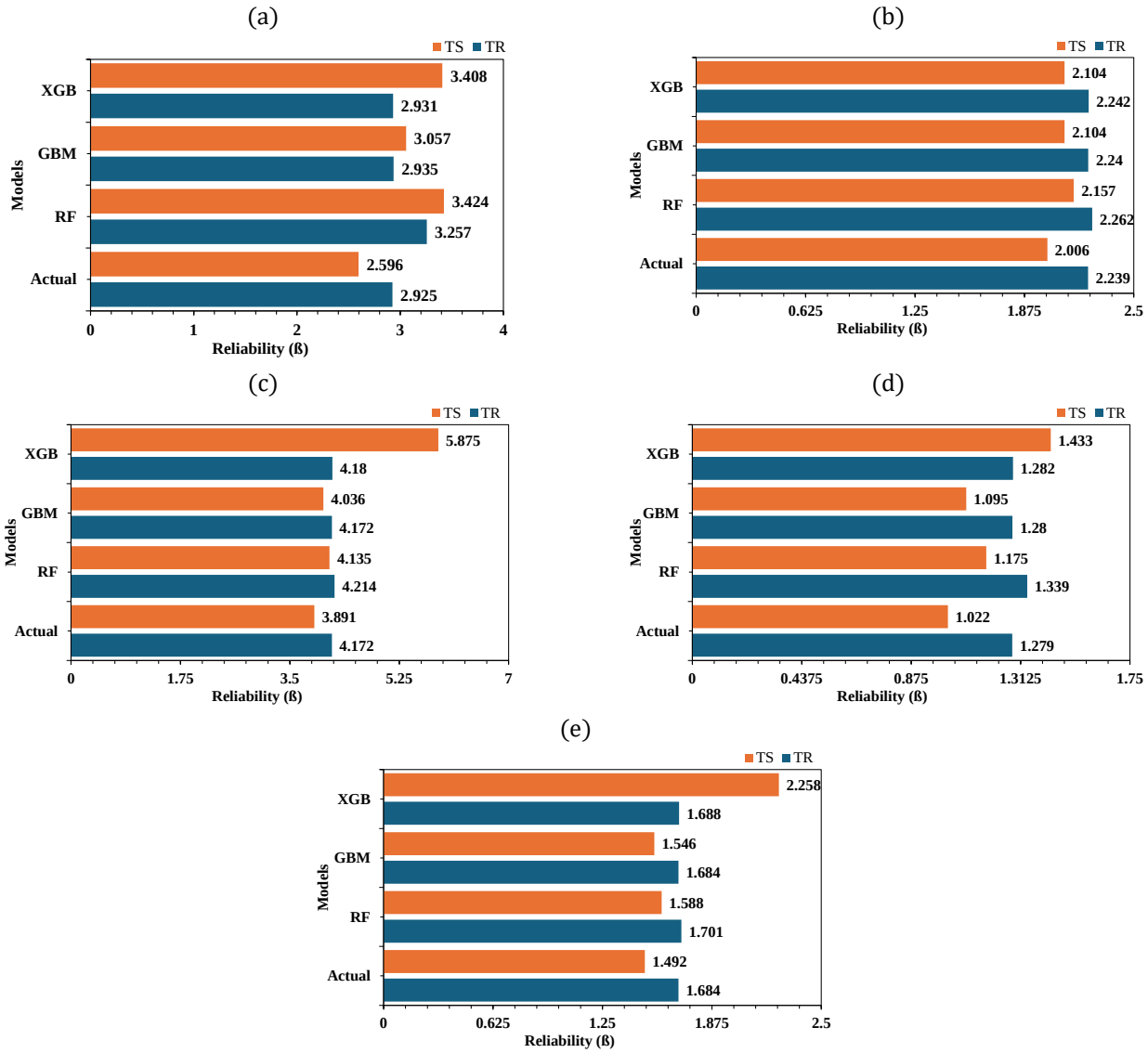

Fig. 6 Bar chart illustrating the reliability indices of the implemented models for each scenario: (a) Rupture, (b) Pullout, (c) Sliding, (d) Bearing Pressure, and (e) Overturning

system's reliability index. A concise version of this calculation is shown in Fig. 7, where the reliability index for the geotextile-reinforced retaining wall system is $\beta_{system} = 1.083$.

It is important to note that the calculations presented above are based on the complete dataset, prior to splitting. A similar approach was followed to split the datasets, where the actual and predicted values for both the training (TR) and testing (TS) conditions were analyzed. The results for the predicted and actual datasets are discussed and illustrated in the subsequent section.

4.4 Comparative assessment in system reliability analysis

Following the above calculations, a similar approach has been used for TR and TS datasets. Based on the results presented in Table 8, a comparison of the system reliability across different models (RF, GBM, XGB) and the actual data reveals some notable insights. In the TR, the actual reliability index (β_{Actual}) is 1.012. The RF model shows a β of 1.010, which is very close to the actual value, indicating that the model performs well in predicting system reliability. Similarly, the GBM model produces a β of 1.005, slightly lower than the actual value, but still quite close, suggesting that the model's performance is acceptable. The XGB model, on the other hand, achieves a β of 1.012, which perfectly matches the actual value, making it the most accurate in predicting system reliability during the training phase. In the TS, the actual reliability index is 1.018. The RF model shows a β of 1.084, which is slightly higher than the actual value, indicating a minor overestimation of the system's reliability in the testing phase. Similarly, the GBM model produces a β of 1.102, which is also higher than the actual value, suggesting a more significant overestimation compared to RF. The XGB model, however, shows a β of 0.974, which is lower than the actual value, indicating an underestimation of the system's reliability in the testing phase

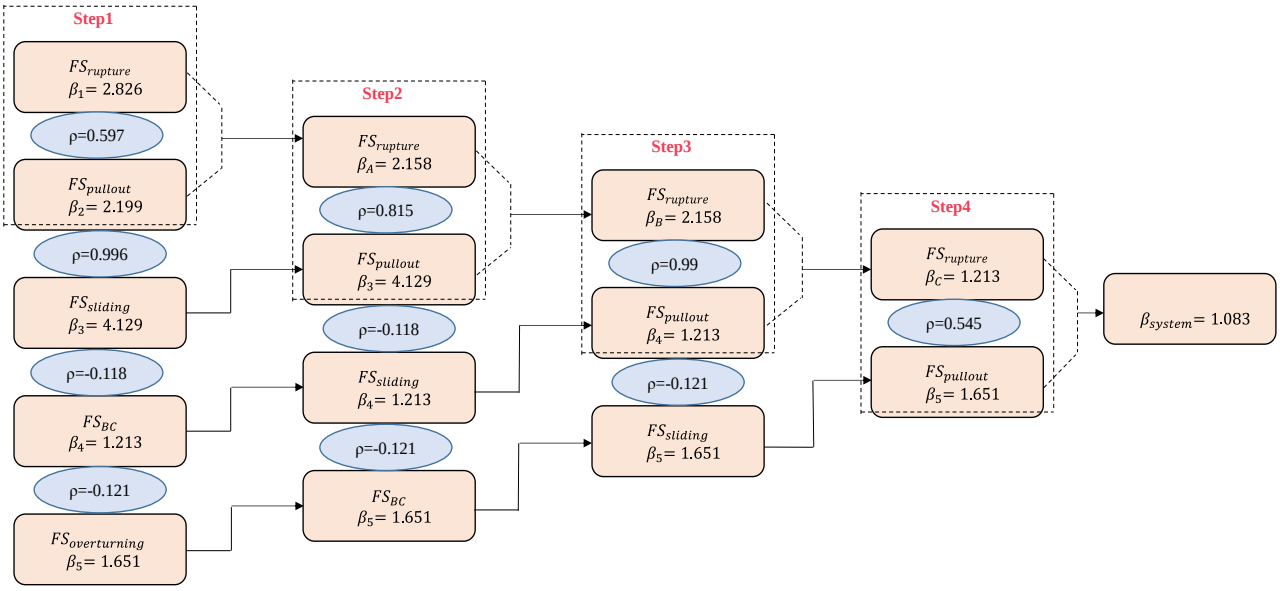

Fig. 7 A system of correlated series for performing the reliability analysis of the geotextile-reinforced retaining wall

Table 8 Comparative Analysis of Actual and Predicted datasets for System Reliability

	Scenario	TR	TS
β_{System}	β_{Actual}	1.012	1.018
	β_{RF}	1.010	1.083
	β_{GBM}	1.005	1.102
	β_{XGB}	1.012	0.974

5. Discussion

The present study successfully combines soft computing techniques (RF, GBM, and XGB) with system reliability methods to evaluate the stability of geosynthetic retaining structures. The results showcase the potential of these advanced approaches in addressing the inherent uncertainties and complexities associated with geotechnical problems. The comparative analysis of machine learning models highlights the robust predictive capabilities of RF and GBM, which consistently outperformed XGB in terms of accuracy and reliability indices. This observation underscores the suitability of ensemble learning techniques like RF and GBM for modelling geotechnical parameters, where input variables such as soil friction angle, soil unit weight, and geotextile tensile strength often exhibit significant variability. The study reinforces the importance of integrating deterministic and stochastic analyses for geotechnical stability evaluations. Traditional deterministic methods, which rely on fixed input parameters, often fail to account for the variability and randomness in soil properties. By incorporating system reliability techniques, the study provides a more comprehensive and probabilistic assessment of structural safety, capturing potential failure scenarios under various conditions (sliding, overturning, bearing capacity, rupture and pullout).

6. Conclusions

This study demonstrates the use of machine learning algorithms and analytical system reliability analysis for geotextile-reinforced retaining walls. In this approach, all stability criteria for such walls, including both external and internal stability, are evaluated, with soil parameters treated as random variables and geometric parameters assumed to be deterministic. The key findings can be summarized as follows:

- Among the machine learning models employed, RF and GBM demonstrated superior predictive performance in estimating FS and β across all failure scenarios sliding, overturning, bearing capacity, rupture, and pullout. Their R^2 values consistently exceeded 85%, with accuracy levels surpassing 90%, affirming their reliability. Additionally, both RF and GBM exhibited lower RMSE and RSR values, indicating minimal error margins and strong model robustness. Furthermore, the Willmott Index (WI) remained above 0.99 in most cases, demonstrating excellent agreement between predicted and actual values. The Bias Factor values were close to 1.0, ensuring unbiased estimations, while high LMI values reinforced the stability and consistency of RF and GBM across different scenarios. The low TIC and sMAPE values further confirmed their superior generalization ability between training and testing datasets. In contrast, the XGB model exhibited notable variability, particularly in sliding and rupture conditions, where test-phase performance deviated significantly. This was evident from higher RMSE and RSR values, along with lower WI values, suggesting potential overfitting or sensitivity to data distribution.
- The FOSM method effectively quantified the reliability of geosynthetic retaining structures under various failure modes. Machine learning models (RF, GBM, and XGB) demonstrated robust performance, providing

reliable predictions with minimal discrepancies between training and testing phases, showcasing the potential of soft computing in geotechnical reliability analysis.

- The incorporation of system reliability methods allowed for a comprehensive probabilistic assessment, considering multiple failure modes such as sliding, overturning, bearing capacity, rupture, and pullout. The system reliability analysis reveals that the GBM model provides the most accurate predictions during the TR and TS phase, while Random Forest and XGB also perform quite well. However, XGB discrepancies in the testing phase suggest varying model performances, emphasizing the need for model refinement in different conditions.
- The system reliability index (βsystem=1.083) was found to be lower than the minimum reliability index (βmin=1.213) obtained from the FOSM analysis of the individual components.

References

Ali, T., Haider, W., Ali, N. and Aslam, M. (2022), "A machine learning architecture replacing heavy instrumented laboratory tests: In application to the pullout capacity of geosynthetic reinforced soils", *Sensors*, **22**(22), 8699. https://doi.org/10.3390/s22228699.

Ardah, A., Abu-Farsakh, M. and Voyiadjis, G. (2021), "Numerical parametric study of geosynthetic reinforced soil integrated bridge system (GRS-IBS)", *Geotext Geomembranes*, **49**, 289-303. https://doi.org/https://doi.org/10.1016/j.geotexmem.2020.10.005.

Bardhan, A., GuhaRay, A. and Gupta, S. (2022), "A novel integrated approach of ELM and modified equilibrium optimizer for predicting soil compression index of subgrade layer of dedicated freight corridor", *Transp. Geotech*., **32**, 100678. https://doi.org/10.1016/j.trgeo.2021.100678.

Bathurst, R.J. and Naftchali, F.M. (2021), "Geosynthetic reinforcement stiffness for analytical and numerical modelling of reinforced soil structures", *Geotext Geomembranes*, **49**, 921-940. https://doi.org/https://doi.org/10.1016/j.geotexmem.2021.01.003.

Berg, R.R., Samtani, N.C. and Christopher, B.R. (2009), "Design of mechanically stabilized earth walls and reinforced soil slopes", Volume II, United States, Department of Transportation, Federal Highway Administration. https://rosap.ntl.bts.gov/view/dot/49730/dot_49730_DS1.pdf.

Breiman, L. (2001), "Random forests", *Mach. Learn*., **45**, 5-32. https://doi.org/10.1023/A:1010933404324.

Chandwani, V., Agrawal, V. and Nagar, R. (2013), "Applications of soft computing in civil engineering: a review", *Int. J. Comput. Appl.*, 81.

Chang, Y.C., Chang, K.H. and Wu, G.J. (2018), "Application of eXtreme gradient boosting trees in the construction of credit risk assessment models for financial institutions", *Appl. Soft Comput*., **73**, 914-920. https://doi.org/https://doi.org/10.1016/j.asoc.2018.09.029.

Chen, R.H., Wu, C.P., Huang, F.C. and Shen, C.W. (2013), "Numerical analysis of geocell-reinforced retaining structures", *Geotext Geomembranes*, **39**, 51-62. https://doi.org/https://doi.org/10.1016/j.geotexmem.2013.07.003.

Chien-Ta, C., Shing-Wen, T., Hsiao, L.H. (2024), "Estimating deformation of geogrid-reinforced soil structures using hybrid LSSVR analysis", *Int. J. Geosynth. Gr. Eng*., **10**, 6. https://doi.org/10.1007/s40891-023-00515-1.

Das, B.M. and Sivakugan, N. (2010), "Principles of foundation engineering", McGraw-Hill handbooks xvii, 595.Ding, Z., Nguyen, H., Bui, X.N., Zhou, J. and Moayedi, H. (2020), "Computational intelligence model for estimating intensity of blast-induced ground vibration in a mine based on imperialist competitive and extreme gradient boosting algorithms", *Nat. Resour. Res*., **29**, 751-769. https://doi.org/10.1007/s11053-019-09548-8.

Djabri, M. and Benmebarek, S. (2016), "FEM analysis of back-to-back geosynthetic-reinforced soil retaining walls", *Int. J. Geosynth. Gr. Eng*., **2**, 26. https://doi.org/10.1007/s40891-016-0067-1.

Elias, V., Christopher, B.R., Berg, R.R. and Berg, R.R. (2001), "Mechanically stabilized earth walls and reinforced soil slopes: design and construction guidelines (updated version)", United States, Federal Highway Administration, FHWA-NHI-00-043. https://rosap.ntl.bts.gov/view/dot/48689/dot_48689_DS1.pdf.

Genz, A. (2004), "Numerical computation of rectangular bivariate and trivariate normal and t probabilities", *Stat. Comput*., **14**, 251–260. https://doi.org/10.1023/B:STCO.0000035304.20635.31.

Gholampour, A. and Johari, A. (2019), "Reliability-based analysis of braced excavation in unsaturated soils considering conditional spatial variability", *Comput. Geotech*., **115**, 103163. https://doi.org/10.1016/j.compgeo.2019.103163.

Goswami, A., Deka, S. and Chakraborty, A. (2022), "Deterministic and probabilistic analysis of effects of fibre reinforcement on strength and deformation of soil—a state-of-the-art review", (Eds., Choudhary, A.K., Mondal, S., Metya, S. and Babu, G.L.S.) Advances in Geo-Science and Geo-Structures. Lecture Notes in Civil Engineering, vol 154. Springer, Singapore. https://doi.org/10.1007/978-981-16-1993-9_17.

Hatami, K. and Witthoeft, A.F. (2008), "A numerical study on the use of geofoam to increase the external stability of reinforced soil walls", *Geosynth. Int*., **15**, 452–470. https://doi.org/10.1680/gein.2008.15.6.452.

Hwang, B., Choi, H., Kwon, K., Shin, Y.J. and Kang, M. (2024), "Prediction models of rock quality designation during TBM tunnel construction using machine learning algorithms", *Geomech. Eng*., **38**(5), 507-515. https://doi.org/10.12989/gae.2024.38.5.507.

Jaiswal, A., Sabri, M.S., Verma, A.K. and Singh, T.N. (2024), "Prediction of UCS and BTS under freeze-thaw conditions in the NW himalayan rock mass using petrographic analysis and laboratory testing", *Quat. Sci. Adv*., **15**, 100225. https://doi.org/https://doi.org/10.1016/j.qsa.2024.100225.

Javankhoshdel, S. and Bathurst, R.J. (2016), "Deterministic and probabilistic failure analysis of simple geosynthetic reinforced soil slopes", *Geosynth. Int*., **24**, 14-29. https://doi.org/10.1680/jgein.16.00012.

Jeyaseelan, P.A. and Madhavan, M. (2024), "Application of FEM and artificial intelligence techniques (LRM, RFM & ANN) in predicting the ultimate bearing capacity of reinforced soil foundation", *Buildings*, 14. https://doi.org/10.3390/buildings14082273.

Jitchaijaroen, W., Keawsawasvong, S. and Wipulanusat, W. (2024), "Machine learning approaches for stability prediction of rectangular tunnels in natural clays based on MLP and RBF neural networks", *Intell. Syst. Appl*., **21**, 200329. https://doi.org/10.1016/j.iswa.2024.200329.

Johari, A., Hajivand, A.K. and Binesh, S.M. (2020), "System reliability analysis of soil nail wall using random finite element method", *Bull. Eng. Geol. Environ*., **79**, 2777-2798. https://doi.org/10.1007/s10064-020-01740-y.

Johari, A. and Elyasi, H. (2024), "Analytical system reliability analysis of a geotextile-reinforced retaining wall", *Int. J. Geomech*., **24**(10), 04024231.

https://doi.org/10.1061/IJGNAI.GMENG-9573.

Khosravi-Hajivand, A. and Johari, A. (2024), "Unsaturated soil nailing wall system reliability analysis using random finite element", *Comput. Geotech*., **173**, 106554. https://doi.org/10.1016/j.compgeo.2024.106554.

Johari, A. and Khodaparast, A.R. (2015), "Analytical stochastic analysis of seismic stability of infinite slope", *Soil Dyn. Earthq. Eng*., **79**, 17-21. https://doi.org/10.1016/j.soildyn.2015.08.012.

Johari, A. and Lari, A.M. (2016), "System reliability analysis of rock wedge stability considering correlated failure modes using sequential compounding method", *Int. J. Rock Mech. Min. Sci*., **82**, 61-70. https://doi.org/10.1016/j.ijrmms.2015.12.002.

Johari, A. and Mousavi, S. (2019), "An analytical probabilistic analysis of slopes based on limit equilibrium methods", *Bull Eng. Geol. Environ*., **78**, 4333-4347. https://doi.org/10.1007/s10064-018-1408-1.

Kang, W.H. and Song, J. (2010), "Evaluation of multivariate normal integrals for general systems by sequential compounding", *Struct. Saf*., **32**, 35-41. https://doi.org/10.1016/j.strusafe.2009.06.001.

Kardani, N., Aminpour, M. and Raja, M.N.A. (2022), "Prediction of the resilient modulus of compacted subgrade soils using ensemble machine learning methods", *Transp. Geotech*., **36**, 100827. https://doi.org/10.1016/j.trgeo.2022.100827.

Keykhosropur, L., Soroush, A. and Imam, R. (2012), "3D numerical analyses of geosynthetic encased stone columns", *Geotext Geomembranes*, **35**, 61-68. https://doi.org/10.1016/j.geotexmem.2012.07.005.

Khandelwal, M. and Singh, T.N. (2006), "Prediction of blast induced ground vibrations and frequency in opencast mine: A neural network approach", *J. Sound Vib*., **289**, 711-725. https://doi.org/10.1016/j.jsv.2005.02.044.

Khorsandiardebili, N. and Ghazavi, M. (2022), "Internal stability analysis of geocell-reinforced slopes subjected to seismic loading based on pseudo-static approach", *Geotext Geomembranes*, **50**, 393-407. https://doi.org/10.1016/j.geotexmem.2021.12.001.

Kumar, D.R., Samui, P., Wipulanusat, W., Keawsawasvong, S., Sangjinda, K. and Jitchaijaroen, W. (2023), "Soft computing techniques for predicting penetration and uplift resistances of dual pipelines in cohesive soils", *Engineered Sci*., **24**(7), 897.

Lin, P. and Liu, J. (2017), "Analysis of resistance factors for LFRD of soil nail walls against external stability failures", *Acta Geotech*., **12**, 157-169. https://doi.org/10.1007/s11440-016-0443-y.

Luo, Z. and Das, B.M. (2016), "System probabilistic serviceability assessment of braced excavations in clays", *Int. J. Geotech. Eng*., **10**, 135-144. https://doi.org/10.1179/1939787915Y.0000000021.

Madhavi Latha, G. and Rajagopal, K. (2007), "Parametric finite element analyses of geocell-supported embankments", *Can Geotech. J*., **44**, 917-927. https://doi.org/10.1139/T07-039.

Marani, A. and Nehdi, M.L. (2020), "Machine learning prediction of compressive strength for phase change materials integrated cementitious composites", *Constr. Build. Mater*., **265**, 120286. https://doi.org/10.1016/j.conbuildmat.2020.120286.

Meyerhof, G.G. (1963), "Some recent research on the bearing capacity of foundations", *Can Geotech. J*., **1**, 16-26. https://doi.org/10.1139/t63-003.

Miyata, Y., Bathurst, R.J. and Allen, T.M. (2018), "Evaluation of tensile load model accuracy for PET strap MSE walls", *Geosynth. Int*., **25**, 656-671. https://doi.org/10.1680/jgein.18.00032.

Momeni, E., Yarivand, A., Dowlatshahi, M.B. and Armaghani, D.J. (2021), "An efficient optimal neural network based on gravitational search algorithm in predicting the deformation of geogrid-reinforced soil structures", *Transp. Geotech*., **26**, 100446. https://doi.org/10.1016/j.trgeo.2020.100446.

Mustafa, R., Samui, P. and Kumari, S.. (2023), "Probabilistic analysis of gravity retaining wall against bearing failure", *Asian J. Civ. Eng*., **24**, 3099-3119. https://doi.org/10.1007/s42107-023-00697-z.

Mustafa, R. and Ahmad, M.T. (2024), "Reliability analysis of pile foundation in cohesionless soil using machine learning techniques", *Transp. Infrastruct. Geotech*., **11**, 2671-2699. https://doi.org/10.1007/s40515-024-00391-w.

Nunes, G.B., Portelinha, F.H.M., Futai, M.M. and Yoo, C. (2022), "Numerical study of the impact of climate conditions on stability of geocomposite and geogrid reinforced soil walls", *Geotext Geomembranes*, **50**, 807-824. https://doi.org/https://doi.org/10.1016/j.geotexmem.2022.04.004

Peng, M., Sun, R., Chen, J.F., Rajesh, S., Zhang, L.M. and Yu, S.B. (2020), "System reliability analysis of geosynthetic reinforced soil slope considering local reinforcement failure", *Comput. Geotech*., **123**, 103563. https://doi.org/10.1016/j.compgeo.2020.103563.

Peng, M., Sun, R., Chen, J.F., Zhang, L.M. and Yu, S.B. (2021), "Stochastic seismic analysis of geosynthetic-reinforced soil slopes using the probability density evolution method", *Comput. Geotech*., **140**, 104485. https://doi.org/10.1016/j.compgeo.2021.104485.

Ray, R., Choudhary, S.S. and Roy, L.B. (2022), "Reliability analysis of soil slope stability using MARS, GPR and FN soft computing techniques", *Model Earth Syst. Environ*., **8**, 2347-2357. https://doi.org/10.1007/s40808-021-01238-w.

Sabri, M.S., Jaiswal, A., Verma, A.K. and Singh, T.N. (2024), "Advanced machine learning approaches for uniaxial compressive strength prediction of Indian rocks using petrographic properties", *Multiscale Multidiscip. Model. Exp. Des*., **7**, 5265-5286. https://doi.org/10.1007/s41939-024-00513-4.

Sharma, S., Venkateswarlu, H. and Hegde, A. (2019), "Application of machine learning techniques for predicting the dynamic response of geogrid reinforced foundation beds", *Geotech. Geol. Eng*., **37**, 4845-4864. https://doi.org/10.1007/s10706-019-00945-7.

Sabri, M.S., Ahmad, F. and Samui, P. (2024), "Slope stability analysis of heavy-haul freight corridor using novel machine learning approach", *Model.. Earth Syst. Environ*., **10**, 201-219. https://doi.org/10.1007/s40808-023-01774-7.

Xing, H., Jiang, T. and Hao, P. (2021), "An efficient dominant failure modes search strategy and an extended sequential compounding method of system reliability analysis and optimization", *Comput. Method. Appl. M*., **375**, 113637. https://doi.org/10.1016/j.cma.2020.113637.

Zevgolis, I.E. and Bourdeau, P.L. (2012), "System reliability of cantilever retaining walls with correlated failure modes", *Proceedings of the GeoCongress 2006, Geotechnical Engineering in the Information Technology Age*, 1-6. https://doi.org/10.1061/40803(187)76 .

GC